Macrophages facilitate peripheral nerve regeneration by organizing regeneration tracks through Plexin-B2

Yuhuan Li,[1,2] Sangjo Kang,[2] Dalia Halawani,[2] Yiqun Wang,[1,2] Chrystian Junqueira Alves,[2] Aarthi Ramakrishnan,[2] Molly Estill,[2] Li Shen,[2] Fengtao Li,[1] Xijing He,[1,3] Roland H. Friedel,[2,4] and Hongyan Zou[2,4]

[1]Department of Orthopedics, the Second Affiliated Hospital of Xi'an Jiaotong University, Xi'an, Shaanxi 710004, China; [2]Nash Family Department of Neuroscience, Friedman Brain Institute, Icahn School of Medicine at Mount Sinai, New York, New York 10029, USA; [3]Department of Orthopedics, Xi'an International Medical Center Hospital, Xi'an, Shaanxi 710065, China; [4]Department of Neurosurgery, Icahn School of Medicine at Mount Sinai, New York, New York 10029, USA

The regeneration of peripheral nerves is guided by regeneration tracks formed through an interplay of many cell types, but the underlying signaling pathways remain unclear. Here, we demonstrate that macrophages are mobilized ahead of Schwann cells in the nerve bridge after transection injury to participate in building regeneration tracks. This requires the function of guidance receptor Plexin-B2, which is robustly up-regulated in infiltrating macrophages in injured nerves. Conditional deletion of Plexin-B2 in myeloid lineage resulted in not only macrophage misalignment but also matrix disarray and Schwann cell disorganization, leading to misguided axons and delayed functional recovery. Plexin-B2 is not required for macrophage recruitment or activation but enables macrophages to steer clear of colliding axons, in particular the growth cones at the tip of regenerating axons, leading to parallel alignment postcollision. Together, our studies unveil a novel reparative function of macrophages and the importance of Plexin-B2-mediated collision-dependent contact avoidance between macrophages and regenerating axons in forming regeneration tracks during peripheral nerve regeneration.

[*Keywords*: peripheral nerve injury; axon regeneration; macrophages; Schwann cells; contact repulsion; collision guidance; Plexin-B2]

Supplemental material is available for this article.

Received September 26, 2021; revised version accepted January 5, 2022.

The regenerative capacity of peripheral nerves (PNs) is unparalleled in the mammalian nervous system. After nerve transection injury, a gap is formed due to retraction of elastin fibers in the two nerve stumps. New tissue formation ensues by first building a nerve bridge consisting of various cell types, including immune cells, Schwann cells, vascular cells, and fibroblasts, as well as extracellular matrix (ECM). The regenerating axons are then guided across the nerve bridge by following regeneration tracks (Chen et al. 2019). Schwann cell plasticity has long been proposed to be instrumental for building the regeneration tracks with longitudinally aligned Schwann cells, termed "bands of Büngner" (Navarro 2009). The role of other cell types in the formation of regeneration tracks and how they interact with regrowing axons are less clear.

Nerve injury attracts a large number of macrophages that infiltrate the injury zone within 24 h, arriving earlier than Schwann cells to initiate inflammation and debris clearing (Zigmond 2012; Liu et al. 2019). Recent studies have revealed important contributions of macrophages for PN regeneration. For instance, one study showed that macrophages are an important source of VEGF to promote angiogenesis at the injury site, and that macrophage-induced blood vessels may serve as tracks to direct Schwann cell migration across the nerve bridge (Cattin et al. 2015). In another study, it was demonstrated that macrophages residing at the outer rim of the nerve bridge secrete Slit3, a repulsive signal that prevents ectopic migration of Schwann cells out of the nerve bridge via Robo1 receptor (Dun et al. 2019). The current investigation builds on these earlier studies to further understand the reparative function of macrophages after peripheral nerve injury (PNI) by shifting the focus onto how physical contacts between macrophages and other cell types in the nerve bridge contribute to nerve repair and axon pathfinding.

Our laboratory has recently unveiled a novel role of axon guidance molecule Plexin-B2 in regulating microglia

Corresponding author: hongyan.zou@mssm.edu
Article published online ahead of print. Article and publication date are online at http://www.genesdev.org/cgi/doi/10.1101/gad.349063.121.

and macrophages after spinal cord injury (SCI) (Zhou et al. 2020). We showed that activated microglia and macrophages up-regulated Plexin-B2 after SCI; absence of Plexin-B2 resulted in failure of glial cells to corral the wound, leading to inflammatory spillover and delayed functional recovery after SCI (Zhou et al. 2020). This is one of the first examples of how immune cells take part in cellular organization during wound repair by reactivating developmentally important pathways. Indeed, apart from critical roles in axon wiring and neurodevelopment, plexins and their cognate ligands, the semaphorins, are engaged in a wide range of physiological processes by mediating cell–cell interactions and cytoskeletal dynamics (Zhou et al. 2008). They also exert important regulatory functions in immune activation (Kumanogoh and Kikutani 2013). However, their roles in nerve repair after PNI are less explored.

These new advances prompted us to ask whether Plexin-B2 plays a similar or a different role in neural repair after PNS versus CNS injury. Notably, there are major differences between PNI and SCI: After SCI, microglia and macrophages become confined to necrotic cores surrounded by an astrocytic border, which facilitates debris clearing, inflammatory containment, and matrix compaction. In contrast, after PNI, there are minimal tissue necrosis, glial corralling, and wound compaction; instead, Schwann cells form bands of Büngner to guide axon pathfinding. A fundamental question is why glial cells behave differently after PNS versus CNS injury. Could it be that the regenerating axons, which exhibit robust growth capacity after PNI but more limited growth capacity after SCI, in fact play a role in governing glial cell organization during neural repair?

Here, we set out to understand cellular interactions of macrophages, Schwann cells, and regenerating axons during PN regeneration by focusing on the role of Plexin-B2 in this process. We show that Plexin-B2 is up-regulated in infiltrating macrophages after PNI; conditional deletion of Plexin-B2 in myeloid lineage resulted in disarray of not only macrophages but also ECM and Schwann cells, leading to misguided axons and delayed functional recovery. Mechanistically, we demonstrate that Plexin-B2 enables macrophages to steer clear of elongating axons, in particular growth cones at the tips of regenerating axons, leading to parallel alignment postcollision. Together, our studies unveil a previously underappreciated mechanism of how macrophages organize regeneration tracks by aligning ECM fibers through collision-dependent contact avoidance. Importantly, our data reveal that regenerating axons do not simply follow regeneration tracks in a passive manner, but instead actively participate in building regeneration tracks by interacting with glial cells at the regeneration front.

Results

Plexin-B2 is up-regulated in infiltrating macrophages after sciatic nerve injury

To evaluate Plexin-B2 expression after PNI, we first used a targeted gene trap mouse line that carriers a *lacZ* reporter in the *Plxnb2* locus (Maier et al. 2011). Staining of sciatic nerves with X-Gal at 7 d after crush injury revealed a marked up-regulation of lacZ expression at the injury site, in contrast to the low baseline expression in contralateral sciatic nerves (Fig. 1A).

To determine the main cell type up-regulating Plexin-B2, we performed sciatic nerve transection injury in $Cx3cr1^{GFP}$ mice, a myeloid-specific GFP reporter line (Jung et al. 2000). Immunofluorescence (IF) imaging showed a large influx of macrophages (GFP^+) into the injured nerve at 5 d postinjury (dpi), with ∼95% overlap with cells expressing Iba1 (a myeloid cell marker) or Plexin-B2 (Fig. 1B,C). The baseline expression of Plexin-B2 in the uninjured nerve appeared low (Fig. 1B,C). Time-course analyses revealed that the peak induction of Plexin-B2 in the injured nerve occurred at ∼5 dpi, a time point of maximal macrophage infiltration into the nerve bridge after transection injury (Fig. 1D,E).

The absence of Plexin-B2 in macrophages disrupts spatial organization of regenerating axons

To investigate the functional significance of Plexin-B2 up-regulation in infiltrating macrophages during nerve repair, we generated tamoxifen-inducible Plexin-B2 conditional knockout (cKO) mice by crossing a floxed allele of *Plxnb2* to the myeloid-specific Cx3cr1-CreER line (Zhou et al. 2020). As macrophages continue to infiltrate the injured nerve, we administrated tamoxifen from 3 d before until 3 d after sciatic nerve lesion (SNL) to ensure Plexin-B2 ablation in the myeloid cell population (Fig. 1F), which was confirmed by IF staining (Fig. 1G,H). Notably, by 5 dpi after transection injury, both control and mutant mice successfully formed a tissue bridge connecting the proximal and distal nerve stumps (Supplemental Fig. S1A). Plexin-B2 deletion did not seem to affect macrophage infiltration or activation in the injured nerve, as both the abundance of $Iba1^+$ cells and the immunointensity of Iba1 appeared comparable in both cohorts (Fig. 1G,H).

Remarkably, IF for SCG10, a marker of regrowing axons (Shin et al. 2014), showed that lack of Plexin-B2 in macrophages resulted in misalignment of regenerating axons: Whereas in littermate controls, regrowing axon fibers were largely oriented in the same direction as the nerve axis at 5 dpi, in Plexin-B2 cKO mutant mice, a significant number of axons deviated from the nerve axis, with many even in perpendicular orientation, giving the appearances of swirls (Fig. 2A,B). The expression levels of SCG10 were not significantly altered in Plexin-B2 cKO mice, signifying intact axonal outgrowth but misguidance of axon pathfinding in the nerve bridge.

We next examined the expression of neurofilaments (NF), which are heteromeric bundles of intermediate filaments that provide mechanical strength for axons (Wang et al. 2012; Yuan et al. 2017). By probing for the subunit NF-H, we observed that the regenerating axons in the proximal injury site contained far less NF-H in Plexin-B2 cKO mice than in a control cohort at matching positions, suggesting delayed maturation of regenerating axons in mutants (Fig. 2C,D; Nixon and Shea 1992).

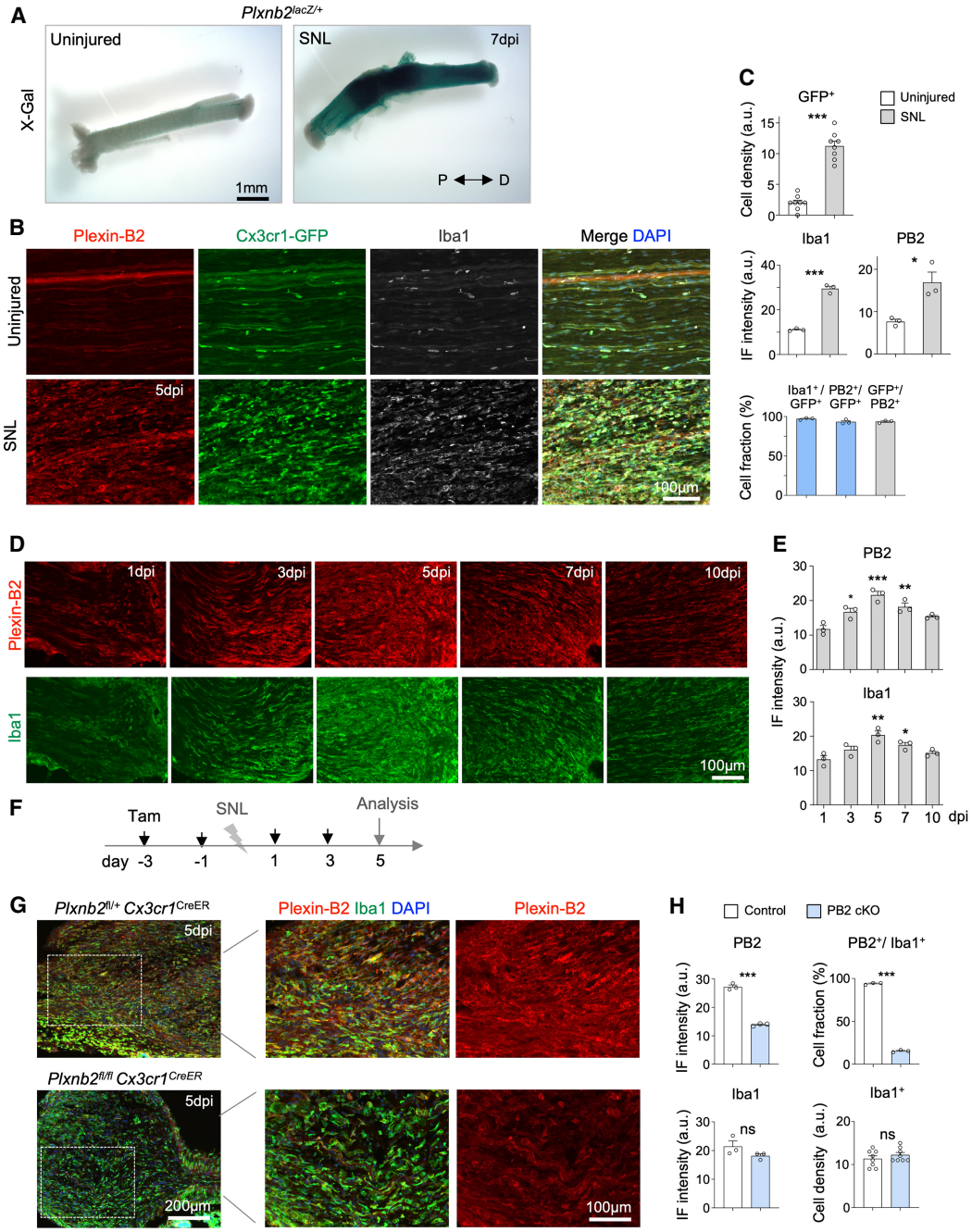

Figure 1. Plexin-B2 is induced in infiltrating macrophages after nerve injury. (*A*) X-Gal staining of sciatic nerves from a mouse line that carriers a *lacZ* reporter in the *Plxnb2* locus reveals increased expression of *Plxnb2*/LacZ at 7 d after crush sciatic nerve lesion (SNL) as compared with uninjured contralateral nerves. Images from $n = 3$ independent mice show similar results. (dpi) Days postinjury, (P) proximal, (D) distal. (*B*) Images of sciatic nerve sections from Cx3xr1-GFP reporter mice after transection SNL show robust infiltration of macrophages (GFP^+) at 5 dpi. Immunofluorescence (IF) staining shows colocalization of Plexin-B2 immunosignals with GFP and macrophage marker Iba1. DAPI was used for nuclear counterstaining. (*C*) Quantifications of the colocalization of Plexin-B2 with GFP and Iba1. $n = 3$ mice. Unpaired two-tailed Student's *t*-test. Bar graphs represent the means ± SEM. (*D*) IF images show robust up-regulation of Plexin-B2 at the injury site after sciatic nerve transection, coinciding with an influx of macrophages ($Iba1^+$). (*E*) Quantifications show peak induction of Plexin-B2 at 5 dpi. $n = 3$ mice per time point. One-way ANOVA with Dunnett's multiple comparisons posttest. (*F*) Experimental scheme for myeloid-specific deletion of Plexin-B2 in an SNL paradigm. Tamoxifen (Tam) was injected from 3 d before until 3 d after SNL to activate CreER recombinase. Analysis was conducted at 5 dpi. (*G*) IF images of sciatic nerves after transection confirm Plexin-B2 ablation in $Iba1^+$ cells of Plexin-B2 cKO mice ($Plxnb2^{fl/fl}$ Cx3cr1-CreER) as compared with littermate controls ($Plxnb2^{fl/+}$ Cx3cr1-CreER). Note similar levels of infiltration of $Iba1^+$ cells and Iba1 expression in both groups. (*H*) Quantifications of Plexin-B2 expression and $Iba1^+$ cell infiltration in injured nerves. Unpaired two-tailed Student's *t*-test. (ns) Not significant ($P = 0.18$ for Iba1 intensity, $P = 0.34$ for $Iba1^+$ cell density).

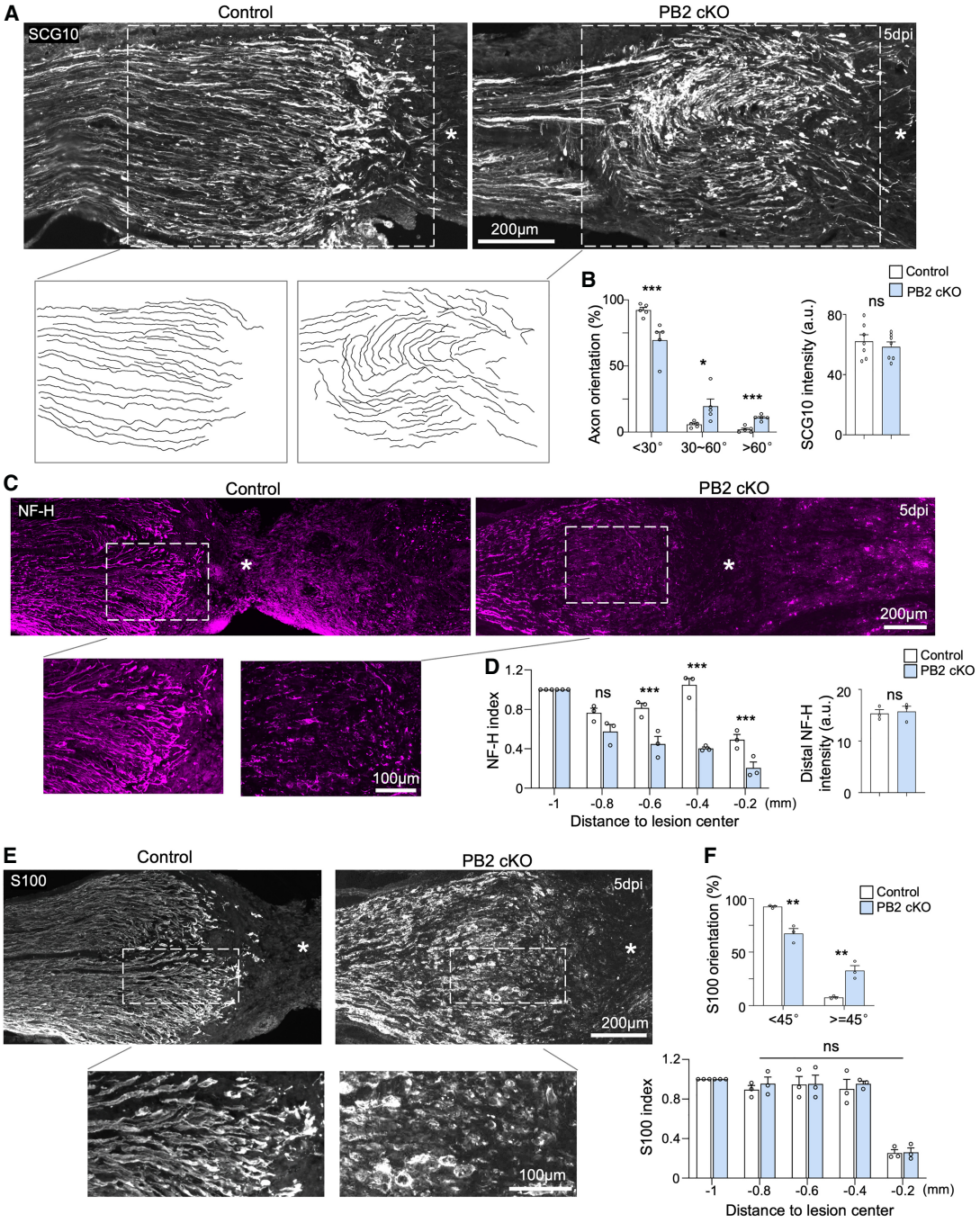

Figure 2. Plexin-B2 ablation in macrophages disrupts sciatic nerve regeneration. (*A*) IF images reveal disorganized regenerating axons (SCG10$^+$) at the proximal injury site at 5 d after sciatic nerve transection in PB2 cKO mice as compared with littermate controls. Tracings of SCG10$^+$ axons are shown *below*. The fluorescence intensity of SCG10 shows no significant differences between conditions. (*B*) Quantifications of axonal orientations demonstrate a higher proportion of misaligned axons in PB2 cKO mice. $n = 5$ pairs of mice. Student's *t*-test. For quantification of SCG10 intensity, $n = 6$ mice per group. Unpaired two-tailed Student's *t*-test. (ns) Not significant ($P = 0.51$). Data represent means ± SEM. (*C*) IF images show less accumulation of neurofilament-H (NF-H) in axons in the proximal injury site in PB2 cKO mice compared with littermate controls. Fluorescence intensities were measured at the indicated distances relative to the lesion center (asterisks) and normalized to the proximal area (−1 mm). (*D*) Quantification of NF-H immunointensity. $n = 3$ mice per group. Two-way ANOVA with Sidak's multiple comparisons test for index. (***) $P < 0.001$, (ns) not signification ($P = 0.08$) at −0.8 mm. Unpaired two-tailed Student's *t*-test for distal intensity. (ns) Not significant ($P = 0.78$). (*E*) IF images reveal disarray of Schwann cells (S100$^+$) at the proximal injury site in PB2 cKO animals. (*F*) Quantification of the orientation of Schwann cells, measured by assessing S100$^+$ fiber direction in relation to nerve axis. $n = 3$ mice for each condition. (**) $P < 0.01$. Unpaired two-tailed Student's *t*-test. For quantification of the S100 index, the fluorescence intensity of S100 was measured at the indicated locations and normalized to the proximal area (−1 mm from lesion center). $n = 3$ mice for each condition. Two-way ANOVA with Sidak's multiple comparisons test.

Interestingly, in the distal stump where Wallerian degeneration takes place (Conforti et al. 2014), we observed similar degenerative patterns of NF-H in both control and cKO cohorts (Fig. 2D). Likewise, the degenerative patterns of myelin in the distal nerve stump also appeared similar in both cohorts, as evidenced by comparable immunointensity and fragmentation of myelin basic protein (MBP) (Supplemental Fig. S1B,C). These observations imply that Wallerian degeneration and myelin debris clearing were not significantly compromised by removal of Plexin-B2 in macrophages.

Schwann cells are known as central organizers of nerve repair after PNI (Parrinello et al. 2010; Rosenberg et al. 2014); we therefore examined their spatial organization in the nerve bridge in our myeloid-specific Plexin-B2 cKO mice. Resonating with the disorganization of regenerating axons in the mutant mice, IF staining for Schwann cell marker S100 (Gonzalez-Martinez et al. 2003) also revealed marked disarray of Schwann cells in the nerve bridge (Fig. 2E,F). Whereas in control mice, individual Schwann cells in the proximal injury site displayed elongated morphology and longitudinal alignment in the direction of the nerve axis, Schwann cells in Plexin-B2 cKO mice displayed stellate or more rounded morphology and appeared in random orientation relative to the nerve axis. Of note, the migration of Schwann cells out of the nerve stump and into the nerve bridge was not affected, as shown by similar distribution of S100 immunosignals across the injury zones (Fig. 2E,F).

We next used a hemicut model, in which only half of the sciatic nerve is transected, thereby minimizing tissue distortion and variability of cellular alignment within the nerve bridge (Supplemental Fig. S2A). Similar to the phenotypes in the full transection model, regenerating axons were also misguided in the nerve bridge of Plexin-B2 cKO mice, with many fibers in vertical orientation relative to the nerve axis, and Schwann cells also appeared in disarray (Supplemental Fig. S2B–E). Interestingly, when we applied the sciatic nerve crush injury model, regenerating axons were longitudinally aligned in both control and Plexin-B2 cKO conditions (Supplemental Fig. S2F,G). Thus, Plexin-B2 function in macrophages appeared indispensable for nerve repair after full transection and hemicut, two injury models that require new tissue formation, but is not required for tissue organization and axon pathfinding after crush injury, which leaves a continuous connective tissue spanning the injury zones.

Macrophages participate in building regeneration tracks through Plexin-B2

So far, our understanding of the function of macrophages during nerve repair remains limited to inflammation, debris clearing, and support of angiogenesis (Cattin and Lloyd 2016). Our data revealed a previously underappreciated role of macrophages in organizing regeneration tracks. We therefore surveyed the spatial organization of macrophages in the nerve bridge in dependence of Plexin-B2 function. Echoing a recent study (Dun et al. 2019), in control animals, we observed a distinct macrophage heterogeneity at different injury zones with respect to morphology, orientation, and spatial arrangement relative to regenerating/degenerating axons (Fig. 3A,B). Specifically, in areas where regenerating axons had arrived, such as the proximal injury site, macrophages assumed a fusiform morphology and collectively aligned in longitudinal orientation parallel to the regrowing axons, but in areas where regenerating axons had yet to reach, such as the middle segment of the nerve bridge, macrophages displayed stellate morphology and random orientation (Fig. 3A,B). In contrast, in Plexin-B2 cKO mice, macrophages displayed stellate morphology and random orientation in both the proximal injury site and the central nerve bridge (Fig. 3A,B). Measurement of the angles between the main cellular axis of macrophages and the nerve axis showed a clear difference of macrophage alignment in cKO versus control animals in the proximal injury site (Fig. 3A,B). In contrast, macrophage alignment in the distal nerve stump showed no overt differences between genotypes: Both largely aligned along the old nerve tracks (Supplemental Fig. S3A,B).

As quantified in Figure 1H, Iba1 expression levels and the distribution of $Iba1^+$ cells in the injury zone appeared unchanged with Plexin-B2 cKO. Plexin-B2 deletion also did not affect macrophage proliferation or expression of phagocytic marker CD68 (Chistiakov et al. 2017) across the injury zones, including both proximal and distal injury sites (Supplemental Fig. S3C,D).

To further evaluate the impact of Plexin-B2 cKO on the organization of regeneration tracks, we examined the distribution of ECM in the nerve bridge. We first surveyed the patterns of reticulin, which is a connective tissue fiber mainly composed of collagen III (Kuter et al. 2007), and of tenascin-C (TNC), which is typically expressed in injured and inflamed tissue (Goh et al. 2010). Consistent with the disorganization of macrophages and Schwann cells in Plexin-B2 cKO mice, both reticulin and TNC were in disarray in the proximal injury site, despite no significant changes of their expression levels (Fig. 3C–F). In contrast, in the distal nerve stump, reticulin fibers appeared similarly aligned along the degenerating tracks in both control and mutant mice (Fig. 3C,D). We also conducted second harmonic generation (SHG) microscopy to assess the architecture of collagen I fibers (Chen et al. 2012). Results revealed that mutant mice displayed a highly disorganized collagen pattern in the proximal but not distal injury site compared with control mice (Supplemental Fig. S4A). As ECM can maintain tracks left behind by migrating cells (Li et al. 2017), these phenotypes signify that Plexin-B2 deficiency in macrophages affects the way ECM proteins are deposited or remodeled in the regeneration tracks, likely due to misdirected macrophage movement inside the nerve bridge.

A recent study reported that macrophage-derived VEGF-A can induce polarization of vasculature within the nerve bridge in a rat PNI model (Cattin et al. 2015). We therefore examined vessel orientation in our mouse PNI model. In both control and Plexin-B2 cKO mice, vasculature in the nerve bridge appeared highly engorged and tortuous, with no apparent differences of vessel

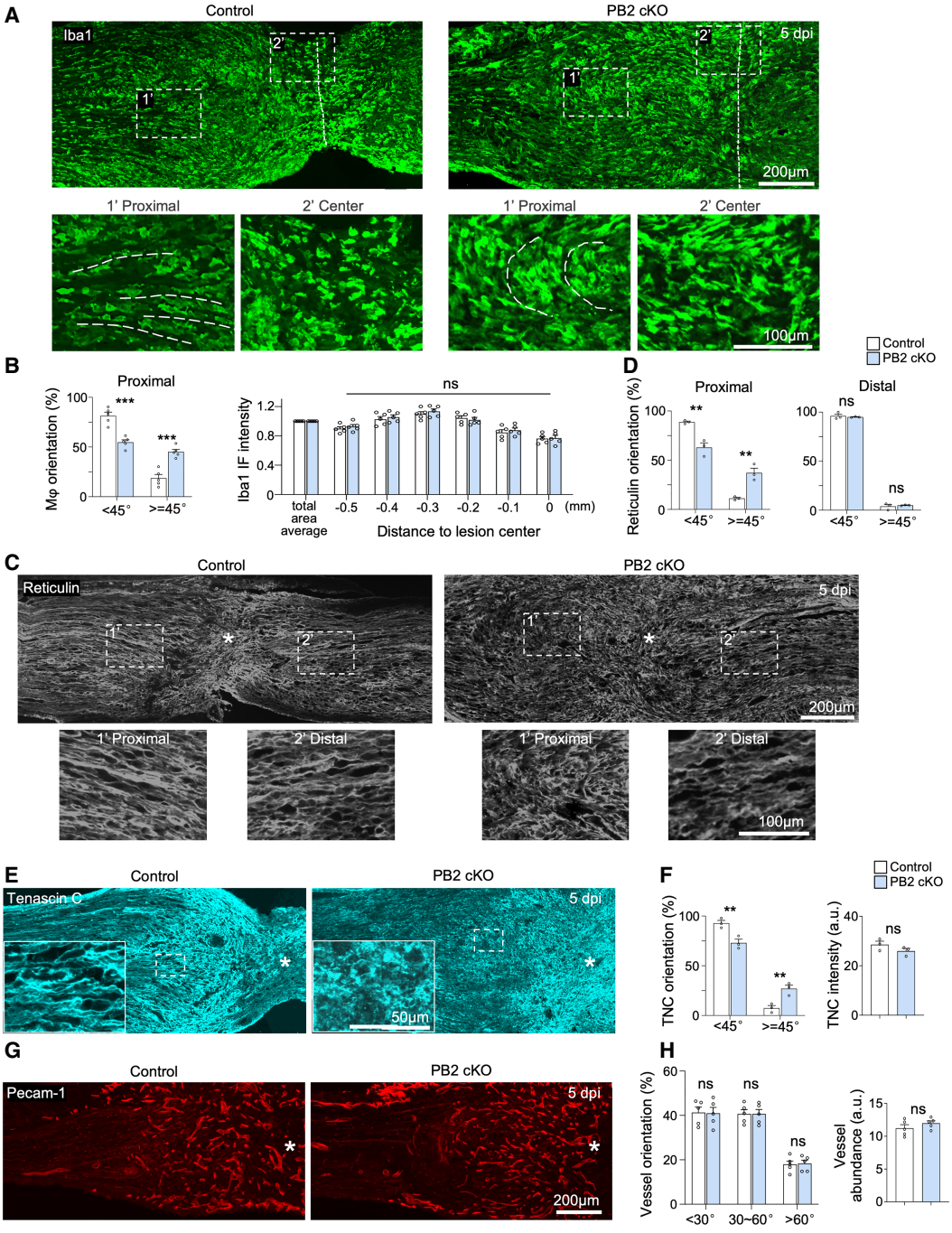

Figure 3. Plexin-B2 cKO results in macrophage misalignment and ECM disorganization during PN repair. (*A*) IF images show misaligned macrophages (Mφ) at the proximal injury site of sciatic nerves in PB2 cKO mice as compared with littermate controls at 5 dpi after nerve transection. Dashed lines in magnified images *below* indicate cell arrangement. Note that in the center of the nerve bridge, the orientation of macrophages appeared random in both cohorts. (*B*) Quantifications show that the distribution of macrophages was not affected by Plexin-B2 cKO, as evidenced by similar Iba1 IF intensities across the injury zones, normalized to the average of the total area. Macrophage alignments were measured in $n = 50$–80 cells per animal, from $n = 5$ pairs of mice. Unpaired two-tailed Student's *t*-test. (***) $P < 0.001$. For quantification of Iba1 IF intensity, $n = 5$ mice per group. Two-way ANOVA with Sidak's multiple comparisons test. Data represent means ± SEM. (*C*) IF images show disarray of reticulin at the proximal injury site of PB2 cKO mice, but aligned arrangement at distal sites. Asterisks denote the lesion center. (*D*) Quantifications of reticulin alignment. $n = 3$ pairs of mice, Unpaired two-tailed Student's *t*-test. (**) $P < 0.01$, (ns) not significant. (*E*) IF images of tenascin C (TNC) deposition show disorganized orientation in Plexin-B2 cKO mice compared with littermate controls. Total levels of TNC were comparable between groups. (*F*) Quantifications of TNC orientation and IF intensity. $n = 3$ pairs of mice. Unpaired two-tailed Student's *t*-test. (**) $P < 0.01$, (ns) not significant. (*G*) IF images show that the patterns and abundance of vasculature (Pecam-1$^+$) were comparable in both cohorts. (*H*) Quantifications of Pecam-1 orientation and abundance. $n = 5$ pairs. Unpaired two-tailed Student's *t*-test. (ns) Not significant.

orientation between the genotypes (Fig. 3G,H; Supplemental Fig. S4B).

Plexin-B2 regulates macrophage alignment along regenerating axons

As the phenotypes suggest that Plexin-B2 might regulate the way macrophages interact with Schwann cells or regenerating axons during the formation of regeneration tracks, we performed co-IF staining for Iba1, SCG10, NF-H, and S100 in the injury zones (Fig. 4A). Interestingly, we observed that in the nerve bridge connecting the two nerve stumps after transection injury, macrophages were mobilized ahead of Schwann cells. Specifically, at 5 dpi, when migrating Schwann cells had not reached the middle segment of the nerve bridge, numerous blood-borne macrophages had already infiltrated the area. Notably, only in the proximal injury site where macrophages came in close contact with both regenerating axons and Schwann cells did they assume fusiform or elongated

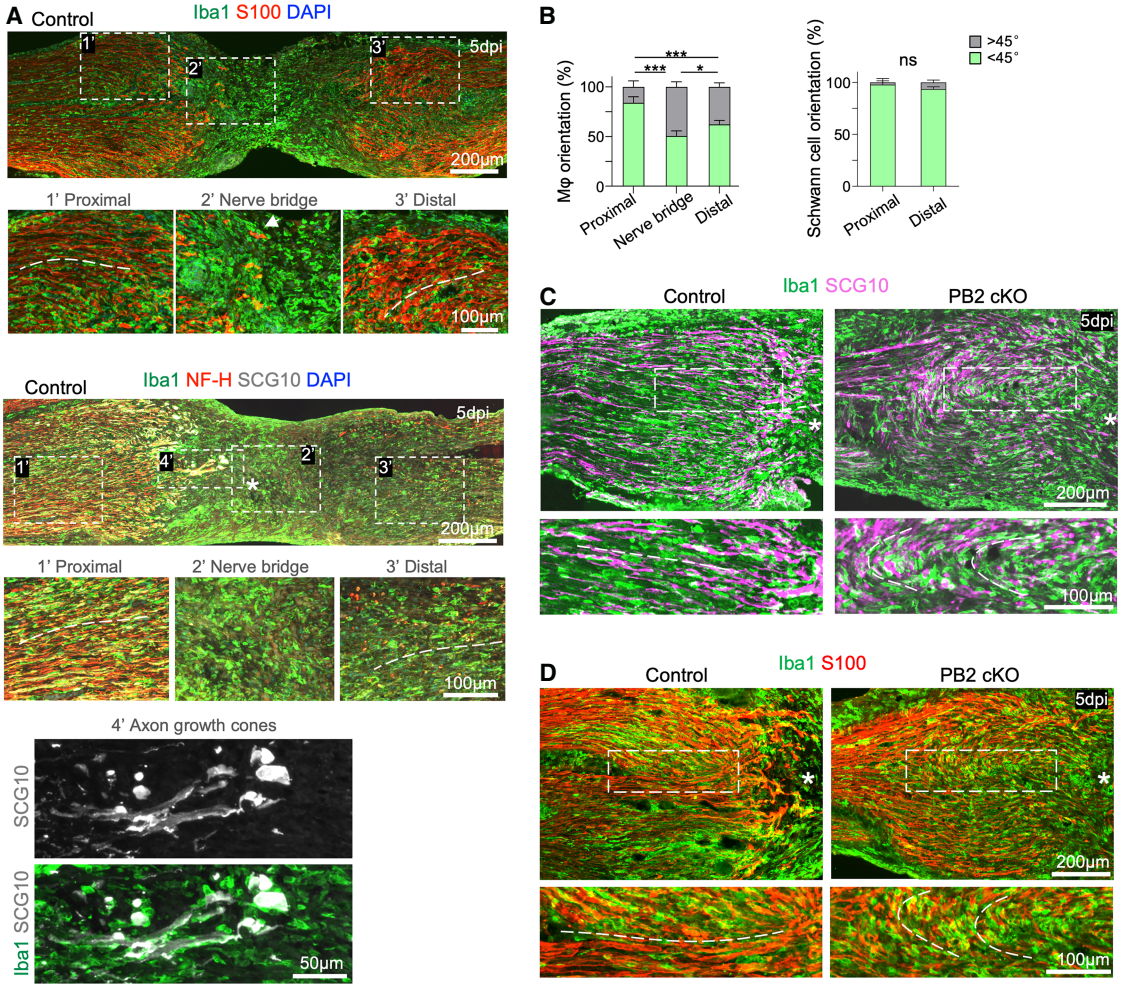

Figure 4. Macrophages are mobilized ahead of Schwann cells in the nerve bridge after transection injury. (*A*) IF images show distinct mobilization and spatial organization of macrophages (Iba1$^+$) and Schwann cells (S100$^+$) across injury zones. At the proximal injury site, both populations extended elongated processes in the same orientation parallel to the regenerating axons (SCG10$^+$). In the center of the nerve bridge, only macrophages had infiltrated the area, but not Schwann cells. Note that macrophages displayed stellate morphology and random orientation. At the distal injury site, both populations appeared elongated and aligned along the nerve tracks left by Wallerian degeneration. Dashed lines in the *bottom* images denote cell alignment along the nerve axis. Maturing axons at the proximal injury site are visualized by NF-H; at the distal injury site, Wallerian degeneration is evidenced by a punctate pattern for NF-H. (*Bottom* panel) Enlarged images highlight the intimate association of the growth cones with macrophages at the regeneration front, with both starting to align in the direction of nerve axis. (*B*) Quantifications of the orientations of macrophages and Schwann cells. For macrophage orientation, $n = 50$–80 cells for each animal, $n = 3$ per cohort; for Schwann cells, $n = 20$–30 S100$^+$ fibers for each animal, $n = 3$ mice per cohort. Two-way ANOVA with Sidak's multiple comparison correction. (*) $P < 0.05$, (***) $P < 0.001$, (ns) not significant ($P = 0.23$). (*C*) IF images show disarray of macrophages (Iba1$^+$) and regenerating axons (SCG10$^+$) in Plexin-B2 cKO at the proximal injury site at 5 dpi after sciatic nerve transection. Similar results were observed in five independent pairs of mice. (*D*) IF images show disorganization of macrophages (Iba1$^+$) and Schwann cells (S100$^+$) in the proximal injury site at 5 dpi in Plexin-B2 cKO mice. Similar results were observed in three independent pairs of mice,

morphologies and align longitudinally in parallel to the nerve axis. In contrast, at the center of the nerve bridge devoid of Schwann cells or regenerating axons, macrophages displayed stellate shape and random orientation (Fig. 4A,B; Supplemental Fig. S5A,B), but in the distal nerve stump with Wallerian degeneration, both Schwann cells and macrophages were largely aligned, reflecting the patterns of previous axon tracks (Fig. 4B; Supplemental Fig. S5B). Closer inspection of the regeneration front clearly outlined close physical contacts between macrophages and re-extending axons, in particular the growth cones at the tip, which appeared in juxtaposition with macrophages, with both starting to align in the direction of the nerve axis (Fig. 4A; Supplemental Fig. S5B).

Indeed, macrophage disorganization in Plexin-B2 cKO mice was only evident in the proximal injury site, but not in the central nerve bridge or in the distal nerve stump. Notably, in the proximal injury site, the misguided macrophages were in close spatial proximity to Schwann cells and regenerating axons, with all showing misalignment with many in vertical orientation to the nerve axis (Fig. 4C,D). These disorganization phenotypes in the proximal injury site persisted at day 10 after sciatic nerve transection injury, whereas axonal alignment and glial organization appeared fairly normal beyond the injury site in the distal nerve stump, suggesting that Plexin-B2 engagement in macrophages is not required for tissue organization or axon pathfinding once axons have crossed the bridge and into the territory of old tracks in the distal stump (Supplemental Fig. S6A–C). Altogether, our data support a central role of Plexin-B2 in macrophages for the governance of axonal contact and glial cytoarchitecture in the regeneration tracks during new nerve tissue formation after transection injury.

Plexin-B2 mediates contact repulsion of macrophages from elongating neurites

To understand the mechanisms by which Plexin-B2 enables macrophages to orchestrate the formation of regeneration tracks, we conducted cell culture assays with bone marrow-derived macrophages (BMDMs). IF staining for CD11b and Iba1 confirmed the purity of BMDM cultures (Supplemental Fig. S7A). We first verified effective ablation of Plexin-B2 in BMDMs isolated from Plexin-B2 cKO mice after hydroxytamoxifen (OHT) treatment (Fig. 5A,B). Consistent with in vivo results, the absence of Plexin-B2 (*Plxnb2*$^{-/-}$) in BMDMs did not affect proliferation or induction of phagocytic marker CD68 (Supplemental Fig. S7B,C). Scratch wound closure assays also did not reveal differences between *Plxnb2*$^{-/-}$ and control BMDMs in their ability to migrate into the scratch wound (Supplemental Fig. S7D,E).

We suspected that cell alignments might be affected by Plexin-B2 deficiency; however, in cultures reaching confluence, both control and *Plxnb2*$^{-/-}$ BMDMs appeared randomly oriented (Fig. 5A; Supplemental Fig. S7B). These results indicate that Plexin-B2 deletion does not affect macrophage behaviors in monocultures, echoing the in vivo results of no overt macrophage phenotypes in the central nerve bridge devoid of regenerating axons or Schwann cells.

We next studied the interactions of macrophages with Schwann cells or regenerating axons in coculture systems. Interestingly, coculture of control or *Plxnb2*$^{-/-}$ BMDMs with IMS32, a Schwann cell line (Watabe et al. 1995), showed no overt differences in regard to cell morphology or cellular alignments (Supplemental Fig. S8A). We next introduced regenerating dorsal root ganglia (DRG) neurons to BMDM cultures and examined cellular arrangement 48 h later. Remarkably, in the control cultures, wild-type BMDMs and elongating axons largely avoided each other, but in cultures with *Plxnb2*$^{-/-}$ BMDMs, neurites were often crossed by BMDMs at a frequency twice as high as that of control cells (Fig. 5C,D). To reduce variables in the coculture systems and to highlight the interactions between BMDMs and elongating axons, we used DRG explant cultures, which allowed separation of elongating axons from neuronal cell bodies. While control BMDMs largely avoided elongating neurites from the DRG explants, *Plxnb2*$^{-/-}$ BMDMs were less adept at avoiding colliding neurites (Supplemental Fig. S8B). The rate of neurite outgrowth was not affected, as shown by similar neurite length in cocultures or in DRG neurons exposed to conditioned media from control or *Plxnb2*$^{-/-}$ BMDMs (Fig. 5C,D; Supplemental Fig. S8C), indicating that mutant macrophages did not affect axon outgrowth potential. Altogether, these results support the model that Plexin-B2 enables macrophages to steer clear of elongating axons.

To further understand cell collision behavior as mediated by Plexin-B2, we performed time-lapse imaging. To facilitate visualization of neurites in live-cell videography, we isolated DRG neurons from Thy-1$^{CreER/GFP}$ reporter mice and plated them onto BMDM cultures. In the control condition, 54.3% ± 3.7% of macrophages displayed contact repulsion when encountering DRG neurites, whereas in the Plexin-B2 knockout condition, only 15.7% ± 3.0% of mutant macrophages displayed contact repulsion, with *Plxnb2*$^{-/-}$ macrophages frequently ignoring and migrating across neurites (Fig. 5E,F; Supplemental Movies S1, S2). Furthermore, in control cultures, when macrophages collided with growth cones at the tips of elongating neurites, they not only displayed repulsive behavior, but also tended to change orientation postcollision in a manner that would lead to parallel alignment of growth cones and macrophages. In contrast, in the Plexin-B2 knockout condition, mutant macrophages exhibited a higher probability of ignoring growth cones and continuing their migratory trajectory, leading to random alignment of macrophages in relation to growth cones (Fig. 5G,H; Supplemental Movies S3, S4).

To examine whether neuronal contact induces Plexin-B2 up-regulation in macrophages, we compared Plexin-B2 expression in BMDMs either cultured alone, cocultured with DRG neurons, or exposed to conditioned media from DRG neurons, with all showing comparable levels of Plexin-B2 immunointensity (Supplemental Fig. S8D). Hence, direct contact with regenerating axons is not required to trigger Plexin-B2 induction in macrophages. This agrees with the in vivo finding that Plexin-B2 is

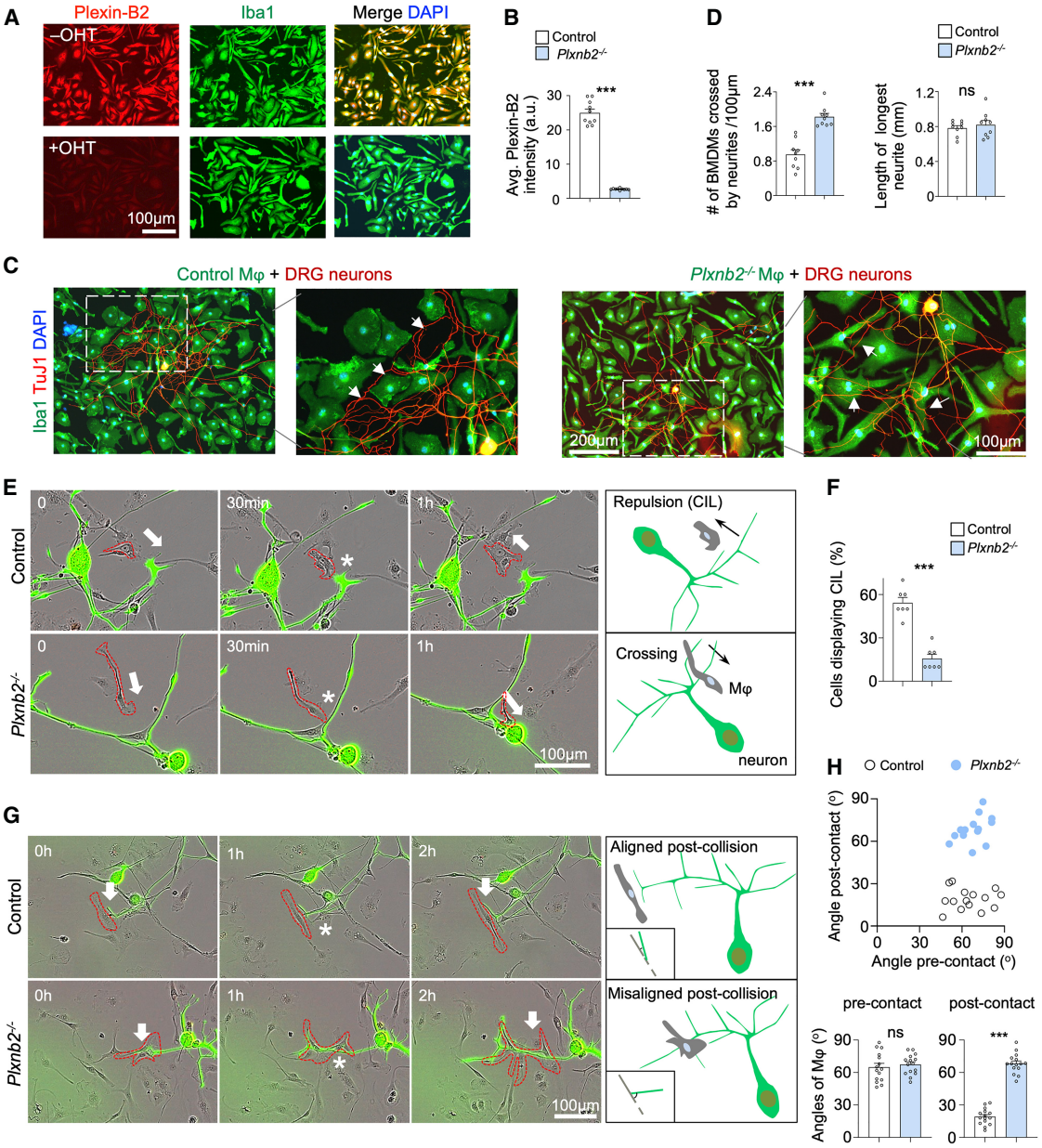

Figure 5. Plexin-B2 provides collision guidance for macrophages upon encountering elongating axons. (*A*) IF images confirm Plexin-B2 ablation in cultured BMDMs (Iba1$^+$) of Plexin-B2 cKO mice after administration of 4OH-tamoxifen (OHT). (*B*) Quantification of Plexin-B2 intensity. $n = 10$ independent batches of cells. Unpaired two-tailed Student's *t*-test. (***) $P < 0.001$. Bar graphs represent the means ± SEM. (*C*) IF Images of cocultured BMDMs (Iba1$^+$) and DRG neurons (Tuj1$^+$) after 48 h. Arrows point to avoidance of elongating axons by control BMDMs, but not by Plexin-B2-deficient BMDMs. (*D*) Quantifications demonstrate an increased fraction of Plexin-B2-deficient BMDMs crossing the elongating axons in cocultures. Note that axon growth was not affected, as the lengths of the longest neurites of DRG neurons were similar in both conditions. $n = 9$ independent batches of cocultures. Unpaired two-tailed Student's *t*-test. (***) $P < 0.001$. (*E*, *left*) Frames from time-lapse live-cell videography of GFP$^+$ DRG neurons from *Thy-1*$^{CreER/GFP}$ mice cocultured with BMDMs from Plexin-B2 cKO mice with or without 4OH-tamoxifen treatment. Arrows point to colliding BMDMs, which moved away upon contact with neurites in control conditions, but not in Plexin-B2 deletion conditions. Asterisks denote contact points. (*Right*) Schematic depiction of contact–repulsion or contact inhibition of locomotion (CIL) of macrophages in control conditions, but not in Plexin-B2 deletion conditions. (*F*) Quantification demonstrates reduced CIL behavior of Plexin-B2-deficient BMDMs compared with controls. $n = 7$ independent cultures, and for each culture, 10 macrophages that had contact with the middle segment of neurites from random views were quantified. Unpaired two-tailed Student's *t*-test. (***) $P < 0.001$. (*G*, *left*) Frames from videography of cocultured BMDMs and DRG neurons. Note the parallel alignment of the growth cones and macrophages postcollision (arrows) in control cultures, but not in Plexin-B2 deletion cultures. Asterisks denote contact points. (*Right*) Schematics of collision guidance for alignment of colliding macrophages and growth cones. (*H*) Quantifications show angles between macrophages and elongating neurites before and after contact. $n = 15$ independent fields. (***) $P < 0.001$. Unpaired two-tailed Student's test.

highly expressed in infiltrating macrophages even in areas devoid of regenerating axons, such as the center of the nerve bridge or the distal nerve stump. In contrast, when stimulated with lipopolysaccharides (LPSs), macrophages robustly up-regulated Plexin-B2, similar to microglia (Supplemental Fig. S8E; Zhou et al. 2020).

Put together, collision-dependent avoidance of contact between macrophages and elongating axons as mediated by Plexin-B2, in particular postcollision parallel alignment of macrophages and growth cones, plays a central role in governing ECM organization in the nerve bridge, thus providing the proper substrate for directed Schwann cell migration out of nerve stumps.

Plexin-B2 function in macrophages is required for functional recovery after peripheral nerve injury

To assess whether Plexin-B2 cKO affects functional recovery after SNL, we measured the motosensory performance after sciatic nerve transection injury for up to 31 dpi. Paw prints collected from hindlimbs during ambulation clearly demonstrated a delay of functional recovery in mutant mice, as confirmed by the sciatic functional index (SFI) calculated based on the spatial patterns of paw prints (Fig. 6A,B; Marcolino et al. 2016; Ydens et al. 2020). Specifically, at 1 dpi, the SFI dropped equally for both control and Plexin-B2 cKO animals; but starting from 6 dpi until 31 dpi, the recovery of Plexin-B2 cKO mice was significantly outpaced by that of the control cohort (Fig. 6A,B). For evaluation of tactile sensory function, we conducted von Frey filament assay, which showed a significant delay in the recovery of mechanical sensitivity of hind paws in the mutant cohort (Fig. 6C).

To obtain an overview of the expression patterns of semaphorins and plexins in the setting of nerve injury, we mapped their expression levels by mining the data set of a recent single-cell RNA-seq study on injured peripheral nerves (Supplemental Fig. S9; Kalinski et al. 2020). The results confirmed that *Plxnb2* is highly expressed in macrophages in injured nerves, while cognate ligands, such as *Sema4b* and *Sema4c*, are highly expressed in Schwann cells, and *Sema4d* is highly expressed in macrophages (Supplemental Fig. S10A). IF staining confirmed a robust up-regulation of Sema4D in macrophages that had entered the injured sciatic nerve at 5 dpi (Supplemental Fig. S10B). We also examined single-cell RNA-seq data sets of DRG neurons in control and nerve injury conditions (Wang et al. 2021), which revealed *Sema4b* and *Sema4f* as the highest expressed semaphorins in DRG neurons, with both genes showing up-regulation upon nerve injury (Supplemental Fig. S11A). Among the heterogenous populations of DRG neurons based on their transcriptional signatures and injury responses, three subclusters of DRG neurons showed a robust up-regulation of *Atf3*, a well-known regeneration-associated gene rapidly induced in axotomized DRG neurons after PNI (Supplemental Fig. S11B; Seijffers et al. 2007). Violin plots of the expression patterns of *Sema4b* and *Sema4f* in these three injury-induced subtypes of DRG neurons confirmed their up-regulation after PNI, suggesting that they may serve as potential axon-derived ligands for Plexin-B2 on macrophages in injured nerves (Supplemental Fig. S11C).

Discussion

Peripheral nerve repair after transection injury involves the formation of new tissue that requires an intricate interplay of many cell types. Even though bands of Büngner have long been described, the molecular regulators of cell–cell interactions in the crowded lesion center in orchestrating the building of regeneration tracks remain poorly understood. Previous research has largely focused on Schwann cells as organizers of bands of Büngner; less attention has been paid to the role of macrophages in this process.

The present study highlights the reparative function of macrophages in organizing regeneration tracks. We unveil the importance of collision-dependent contact repulsion as mediated by Plexin-B2 by steering macrophages clear of colliding axons (Fig. 6D). One insight arising from our study is that the regenerating axons do not just passively follow the regeneration tracks laid ahead, but instead actively participate in the physical contacts with macrophages (in particular, the highly dynamic growth cones) in a manner that leads to parallel alignment postcollision. This in turn governs longitudinal matrix alignment, thereby providing the proper substrate for directed Schwann cell migration out of the nerve stump and into the nerve bridge to further fortify the regeneration tracks.

Indeed, the longitudinal alignment of macrophages requires axonal contact and Schwann cell interaction, as macrophages in the center of the nerve bridge devoid of regenerating axons or Schwann cells are stellate-shaped and randomly oriented, but start to realign where they come in close contact with the growth cones of regrowing axons at the regeneration front. We considered the possibility that cellular contacts with Schwann cells might govern organization of macrophages; however, coculture experiments showed that contacts between these two populations did not trigger macrophage alignment. Remarkably, when DRG neurons were introduced into BMDM cultures, live-cell videography revealed that whereas wild-type macrophages are adept at avoiding elongating axons, Plexin-B2-deficient macrophages frequently ignored the elongating neurites and migrated across axons. This phenotype is reminiscent of a phenomenon termed contact inhibition of locomotion (CIL), wherein colliding cells move away from one another. Indeed, CIL has been described for osteoclast/osteoblast interactions via Sema4D and Plexin-B1 (Deb Roy et al. 2017), and our recent study reported CIL behavior of microglia via Plexin-B2 after SCI (Zhou et al. 2020). In the present study, we showed that Plexin-B2 enables macrophages to steer clear of colliding axons, in particular the growth cones, leading to parallel alignment postcollision. Hence, in both SCI and PNI, Plexin-B2 appears to play a similar role in steering myeloid cells away from colliding cells.

However, specific tissue context clearly dictates a distinct outcome: In SCI, repeated CIL resulted in

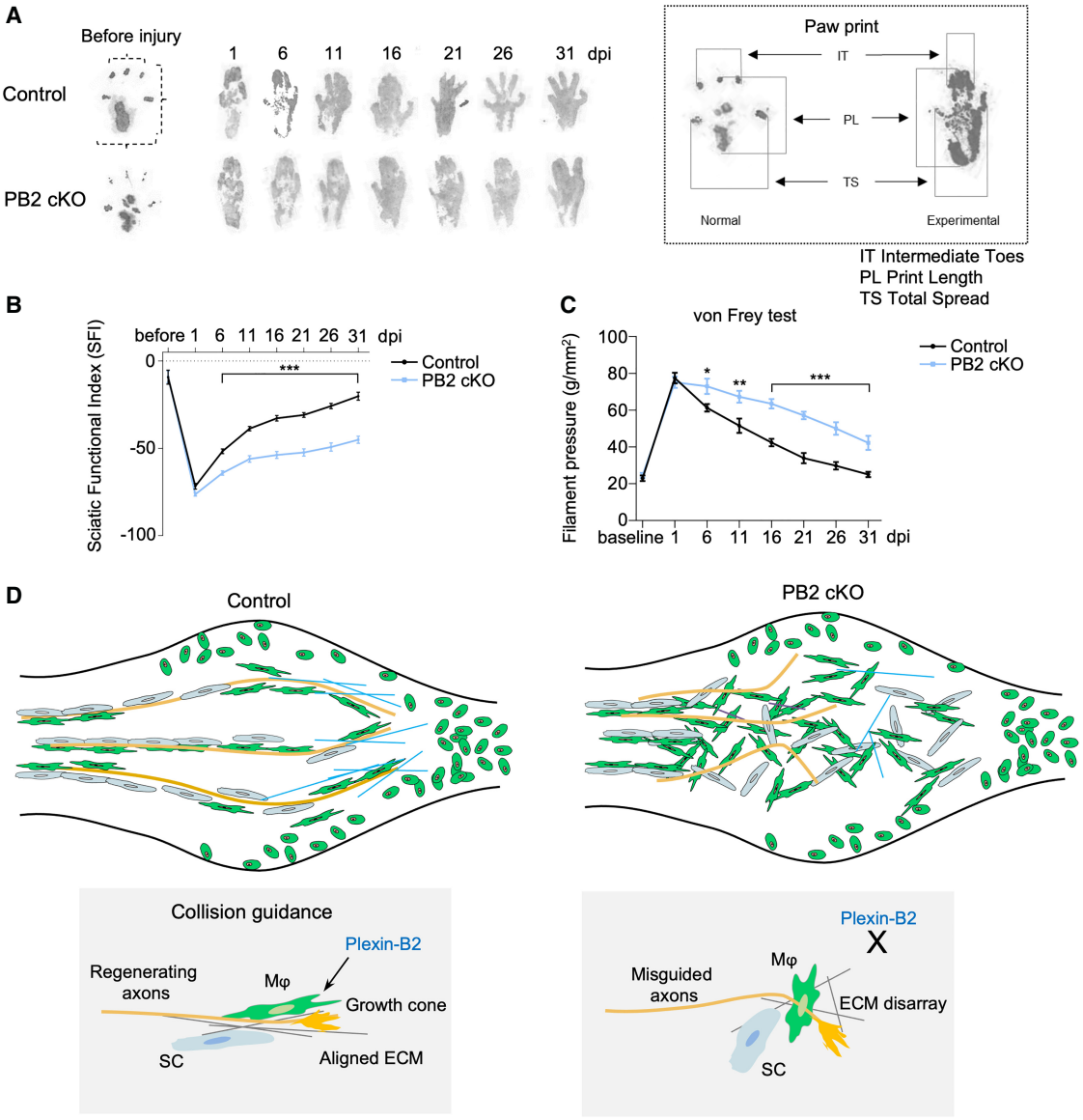

Figure 6. Impaired functional recovery after sciatic nerve injury in Plexin-B2 cKO mice. (*A*) Paw prints were measured to assess the sciatic functional index (SFI) after SNL. Examples of paw prints before and after SNL are shown. The schematic at the *right* illustrates measurement of paw print dimensions (see the Materials and Methods for the formula to calculate the SFI). (*B*) Quantification of the SFI after SNL revealed impaired functional recovery in PB2 cKO mice. $n = 6$ mice for each condition. Two-way ANOVA with Sidak's multiple comparisons test. Data points represent the means with SEM. (*C*) Tactile assay with von Frey filaments shows reduced sensory recovery in PB2 cKO mice after SNL. The *Y*-axis shows calculated filament pressure. $n = 6$ pairs of mice. Two-way ANOVA with Sidak's multiple comparisons test. (*D*) Graphical abstract. Plexin-B2 provides collision guidance for macrophages to steer them clear of colliding growth cones, leading to parallel alignment postcollision. This facilitates alignment of ECM deposition and directed Schwann cell migration to fortify the regeneration tracks. The absence of Plexin-B2 in macrophages in mutant mice resulted in disorganization of macrophages and Schwann cells, as well as misguided axon pathfinding in the regenerating nerve.

confinement of microglia/macrophages in the necrotic core surrounded by astrocytes (Zhou et al. 2020), whereas in PNI, CIL enables macrophages to avoid colliding growth cones, leading to parallel alignment along the nerve axis together with Schwann cells. One stark difference between PNS and CNS is axon regeneration capacity: The highly dynamic growth cones at the tip of regenerating axons after PNI may in fact be a determining factor in providing guidance cues in directing collision-dependent contact avoidance and thereby spatial arrangement of glial cells. In contrast, the dystrophic growth cones in SCI may present poor guidance cues for colliding glial cells. Another interesting difference is that in coculture experiments, astrocytes and microglia are often segregated from one another, reminiscent of the corralling process observed in vivo after SCI (Zhou et al. 2020), but in cocultures of

Schwann cells and macrophages, the two populations remained intermingled. This difference in cell–cell sorting might also contribute to the distinct glial cell arrangements after CNS versus PNS injury, with microglia/macrophages being corralled in the necrotic core by astrocytes in SCI, whereas macrophages and Schwann cells both display longitudinal alignment along regeneration tracks in PNI.

As cells migrate, they leave behind a trail of ECM fibers in the same orientation as the direction of cell movement (Park et al. 2020). We showed here that by removing Plexin-B2 in macrophages, ECM fibers such as reticulin, TNC, and collagen became disorganized in the nerve bridge. Mechanistically, coculture experiments using live-cell videography revealed that Plexin-B2-deficient macrophages are less adept at resolving collision with elongating axons. Together, these data support a connection between Plexin-B2 engagement in macrophages and matrix alignment in the nerve bridge that hinges on collision-dependent avoidance of contact. Remarkably, Schwann cells also appeared highly disorganized in the nerve bridge in Plexin-B2 cKO mutant mice. The Schwann cell phenotype may be secondary to the overall tissue disorganization, as matrix disarray provides an improper substrate for directed Schwann cell migration out of the nerve stump. Our results do not exclude the scenario that both Schwann cells and macrophages might be critical for optimized nerve regeneration. Indeed, earlier studies showed that when Schwann cell proliferation is interrupted, axon regrowth slows down and is misdirected due to insufficient deposition of laminin from Schwann cells (for review, see Zochodne 2012). A previous study using a rat PNI model has reported longitudinal vessel orientation in the nerve bridge on which directed Schwann cell migration occurs (Cattin et al. 2015). In the current study, we found that the vasculature in the nerve bridge appeared highly engorged and tortuous, with no apparent differences of vessel orientation between Plexin-B2 cKO and control cohorts. Whether this reflects species difference requires further study. Future studies using in vivo live imaging of the nerve bridge may further delineate the physical interactions between regrowing axons, glial cells, and vasculatures.

Macrophages up-regulate Plexin-B2 in response to injury cues regardless of transection or crush injury. The ability of macrophages to steer clear of colliding axons through Plexin-B2 seems to be more critical for nerve repair after transection injury than after crush injury. After nerve transection, a new nerve bridge needs to be built—a much more demanding task that requires collision guidance provided by Plexin-B2 to govern longitudinal alignment of ECM and glial cells in forming the regeneration tracks; after crush injury, on the other hand, connective tissues and old tracks remain, and Plexin-B2-mediated contact avoidance is not required, as Plexin-B2-deficient macrophages may use other surface adhesion molecules to align along the old tracks. Notably, the current study focuses on early phase recovery after PNI; whether Plexin-B2 engagement in macrophages is needed for late phase recovery after crush or transection injury to assist myelin remyelination requires further study.

Our study puts Plexin-B2 on the map as a new player in nerve regeneration, thus expanding the list of axon guidance molecules as mediators of cell–cell interactions in the injury setting. Our finding complements a recent report that macrophages in the outermost layer of the nerve bridge restrict ectopic migration of Schwann cells out of nerve bridge through the action of axon guidance molecules Slit3 and Robo (Dun et al. 2019). In the current study, we reveal how macrophages inside the nerve bridge express Plexin-B2 to facilitate the alignment of Schwann cells to fortify longitudinal regeneration tracks.

The identity and cellular source of the ligands for Plexin-B2 remain to be determined. Class 4 semaphorins comprise six family members expressed in diverse cell types (Zhou et al. 2008). For instance, Sema4D is expressed in microglia, oligodendrocytes, and lymphocytes (Gurrapu and Tamagnone 2016). Here we showed that Sema4D is highly up-regulated in macrophages in injured nerves, and that Sema4B and Sema4F may serve as potential axon-derived ligands for Plexin-B2 expressed on macrophages. Intriguingly, a semaphorin-independent function of plexins as mechanosensors of sheer force has recently been reported (Mehta et al. 2020). Conceivably, Plexin-B2 on the cell surface of migrating macrophages may function to sense the compressive forces from colliding growth cones, leading to cytoskeletal reorganization and parallel alignment, mirroring the role of Plexin-D1 in aligning endothelial cells in the direction of blood flow (Mehta et al. 2020). The flexion of the ectodomain of Plexin-D1 is central for mechanosensing function, as a mutant form of Plexin-D1 that is "locked" in a closed ring configuration by an intramolecular disulfide bond loses mechanosensitivity but maintains the capability to bind to semaphorins. Future studies are needed to disentangle the semaphorin-dependent versus semaphorin-independent function of Plexin-B2 by testing a LOCK mutant in the corresponding amino acids.

In sum, our study reveals the mechanisms by which collision guidance provided by Plexin-B2 allow macrophages to steer clear of colliding axons, in particular from highly dynamic growth cones, leading to parallel alignment at the regeneration front, and thereby longitudinal ECM deposition and directed Schwann cell migration to fortify regeneration tracks. Our data highlight the importance of physical contacts and collision guidance in addition to growth factors and biochemical cues for successful nerve repair after peripheral nerve injury.

Materials and methods

Mouse mutants

Plexin-B2 floxed mice were generated in our laboratory (Daviaud et al. 2016) and have been deposited at the Jackson Laboratory as JAX strain 036883 [JAX-MGI allele symbol *Plxnb2*$^{tm1c(EUCOMM)Wtsi}$]. A mouse line expressing CreER from the *Cx3cr1* gene locus (Parkhurst et al. 2013) was obtained from the Jackson Laboratory [JAX 021160; *Cx3cr1*$^{tm2.1(cre/ERT2)Litt}$], as

well as the Cx3cr1-GFP reporter line (JAX 005582; *Cx3cr1*^{tm1Litt}) (Jung et al. 2000). Mice were bred on a C57BL/6J genetic background.

To generate myeloid-specific conditional knockout (cKO) of Plexin-B2, *Cx3cr1*$^{CreER/+}$ *Plxnb2*$^{fl/+}$ mice were bred with *Plxnb2*$^{fl/f}$ mice. The offspring showed an expected 25% probability of *Cx3cr1*$^{CreER/+}$ *Plxnb2*$^{fl/fl}$ genotype. Littermates served as controls.

The CreER recombinase was activated by intraperitoneal (i.p.) injection of tamoxifen (100 mg/kg; Sigma T5648), prepared as stock solution of 20 mg/mL in corn oil (Sigma C8267).

Sciatic nerve injury models

Mice were anesthetized, and a small skin incision was made with a surgical blade at the mid-thigh region. The fascia between the gluteus superficialis and biceps femoris muscles was gently opened to expose the sciatic nerve, and the nerve was carefully freed from surrounding connective tissue. For the sciatic nerve transection model, the nerve was completely cut with a Vannas spring scissor (FST 15000-00) and the cut ends were then returned to their original anatomical position (<2-mm distance between ends). For the sciatic nerve crush model, the nerve was crushed for 15 sec with an ultrafine hemostatic forceps (FST 13021-12), locking the ratchet at the third position. For the hemicut model, the sciatic nerve was transected using the fine scissor only half way, leaving the other half intact. The skin was closed with two suture clips.

X-Gal staining of sciatic nerves

Injured and contralateral sciatic nerves were dissected and fixed for 4 h in 4% paraformaldehyde in PBS. After three washes with PBS, nerves were incubated in staining buffer (0.1 M phosphate buffer at pH 7.3, 2 mM $MgCl_2$, 5 mM potassium ferrocyanide, 5 mM potassium ferricyanide, 0.01% sodium deoxycholate, 0.02% nonidet P-40) containing 1 mg/mL X-Gal (LabScientific) overnight at 37°C.

Culture of bone marrow-derived macrophages (BMDMs)

Femur and tibia bones of hind legs were collected from 6- to 8-wk-old Plexin-B2 cKO mice. The muscles and soft tissue attached to the bones were removed, and the bones were chopped to expose the ends of the marrow cavity. Each bone was clamped with a forceps, and the marrow cavity was flushed out with 2 mL of DMEM (Gibco 10569044) supplemented with 10% FBS (Gibco 10082139) and 1% antibiotic–antimycotic (Gibco 15240062) using a syringe attached to a 25-gauge needle. The suspension was collected and diluted 1:5 before seeding. The growth factor M-CSF (Peprotech 315-02) was added to the medium at 50 ng/mL. Cells were cultured in a 37°C 5% CO_2 incubator and the medium was changed every 2 d. Cells were harvested after they fully differentiated (after 4–6 d). For deletion of Plexin-B2 in cKO cells, macrophages were treated with 4-hydroxytamoxifen (Sigma T176) at 500 ng/mL for 2 d. The 4-hydroxytamoxifen stock solution of 5 mg/mL was prepared in ethanol.

DRG neuron culture

For primary culture of dorsal root ganglion (DRG) neurons, lumbar DRGs from B6 WT mice (6–8 wk old) that had undergone conditional sciatic nerve injury 3 d prior were dissected and placed into ice-cold DMEM/F12 (Gibco 11330057). DRGs were washed three times with HBSS (Gibco 14175-079) containing 1% HEPES buffer (Gibco 15630-106). Collagenase (stock solution 3%; Worthington LS004196) was diluted 1:10 in HBSS buffer with 1% HEPES, and DRGs were incubated for 90 min at 37°C.

DRGs were then washed three times with HBSS containing 1% HEPES, followed by incubation with trypsin (Gibco 25200072) containing 2.5 µg/mL DNase I (Worthington LK003172) for 30 min at 37°C. After digestion, trypsin solution was removed, and warm DMEM with 10% FBS and 2.5 µg/mL DNase I was added to stop the reaction. The solution was triturated ~30 times with fire-polished Pasteur glass pipets. Cell suspension (1 mL) was combined with 8 mL of neurobasal-A (Gibco 10888022), and 2 mL of 15% BSA in PBS was added to the bottom of a 15-mL tube. The solution was centrifuged at 1000 rpm for 6 min. Supernatant was removed, the cell pellet was resuspended in 1 mL of DRG culture medium, and cells were plated into poly-L-ornithine-coated (PLO; Sigma P4957) chamber slides. DRG culture medium consisted of 2% B27 (Gibco A3582801), 0.5 mM L-glutamine (Gibco 25030081), 1% antibiotic–antimycotic, and 0.725% glucose in neurobasal-A.

Coculture of macrophages and DRG neurons

BMDMs (2×10^4 cells/well) were seeded and cultured in PLO-coated four-well chamber slides. After 2 d, primary DRG neurons were introduced into the wells (3000 cells/well). The culture medium was changed to a 1:1 mix of BMDM medium and DRG medium. After another 2–3 d of coculture, cells were fixed and stained.

For DRG explant culture, after collagenase treatment, DRGs were plated on PLO and laminin-coated coverslips in DRG medium. After 2 d, BMDMs were introduced into the DRG explant culture in a 1:1 mix of BMDM medium and DRG medium.

Immunofluorescence staining

For fixation of cells growing in chamber slides, cells were washed gently with PBS, then incubated with fixative (4% paraformaldehyde [PFA; Acros AC416785000] with 4.5% sucrose) for 10 min at room temperature. The slide was washed three times with PBS before staining.

For fixation of mouse tissues, animals were euthanized by injection of pentobarbital (Euthasol), and sciatic nerves at the injury site were dissected, fixed for 2 h in 4% PFA in PBS at 4°C, incubated in 15% and 30% sucrose/PBS each overnight, and embedded in OCT compound (Fisher Health Care 4585) for cryosectioning of 12-µm-thick sections.

For immunofluorescence (IF) staining, slides were washed once with PBS and then incubated with blocking buffer (5% donkey serum [Jackson ImmunoResearch 017-000-121], 0.3% Triton X-100 [Acros 9002-93-1]) in PBS for 1 h at room temperature. After blocking, slides were incubated with primary antibodies (Table 1) diluted in antibody dilution buffer (1% BSA [Fisher BioReagents BP9703100], 0.3% Triton X-100) in PBS overnight at 4°C. Subsequently, slides were washed three times with PBS and then incubated with secondary antibodies conjugated with Alexa fluor 488, 594, or 647 (1:300; Jackson ImmunoResearch) and DAPI for nuclear staining (1:1000; Invitrogen D1306) for 2 h at room temperature. Slides were washed with PBS and the coverglass was mounted with Fluoromount G (Southern Biotech 0100-01).

IF images were captured using a Zeiss Axio Imager.A2 microscope with AxioCam MRm camera. Tiled images were merged using Photoshop CS6. For second harmonic generation (SHG) imaging, 12-µm unstained sections were observed under RXD1 channel (HV: 735 V, gain: 2×, offset: 22%) on an Olympus FV1000 multiphoton microscope.

Table 1. *List of antibodies*

Antibody target	Host	Dilution	Company and catalog number
CD68	Rat	1:200	Bio-Rad MCA1957GA
GFP	Chicken	1:500	Aves Laboratoy GFP-1020
Iba1	Goat	1:125	Novus NB100-1028
Iba1	Rabbit	1:500	Wako 019-19741
Ki67	Rabbit	1:200	Abcam ab15580
NF-H	Chicken	1:1000	EMD Millipore AB5539
MBP	Rabbit	1:50	Cell Signaling 78896
PDGFRβ	Rabbit	1:100	Abcam ab32570
Pecam-1/CD31	Rat	1:250	BD Pharmingen 553370
Plexin-B2	Armenian hamster	1:800	eBioscience eBio3E7
Reticulin	Rat	1:500	Abcam ab51824
S100	Rabbit	1:1000	Dako Z0311
STMN2/SCG10	Rabbit	1:800	Novus NBP1-49461
Tenascin C	Rabbit	1:100	Merck Millipore AB19011
Tubulin β-III/TuJ1	Mouse	1:500	BioLegend 801202
VEGF	Mouse	1:50	Invitrogen MA5-13182

Behavior tests

To measure sciatic nerve function after injury, paw print analysis was performed (Marcolino et al. 2016). Briefly, paws were dipped into ink and mice were allowed to walk on paper to collect paw prints for further analysis.

Paw print dimensions were measured (see Supplemental Fig. S10C), and the sciatic functional index (SFI) was calculated using the formula $SFI = -38.3 \times (EPL - NPL)/NPL + 109.5 \times (ETS - NTS)/NTS + 13.3 \times (EIT - NIT)/NIT - 8.8$, where E is experimental, N is normal, PL is print length, TS is total spread, and IT is intermediate toes.

To assess sensory functional recovery, von Frey assay was performed. Mouse paws were touched with filaments of different strengths (gram). A baseline for the sensitivity of animals was also collected before injury. A lower strength value reflects better sensory functional recovery.

IncuCyte live imaging and videography

To observe the contact behavior of BMDMs and DRG neurons in coculture, primary DRG neurons from Thy-1$^{CreER/GFP}$ mice cocultured with BMDMs in 24-well plates were tracked in an IncuCyte device (Sartorius) by time-lapse live-cell imaging, with images captured every 30 min for 24 h.

To quantify contact inhibition of locomotion (CIL) behavior of cells (Scarpa et al. 2013), the probability of protrusion and retraction of BMDMs after collision with the middle stretch of neurites was determined. The angles between the trajectory of BMDMs and neurites before and after contact were also quantified.

Bioinformatics

The single-cell RNA-seq data sets of control and injured sciatic nerve (Kalinski et al. 2020) and DRG neurons (Wang et al. 2021) were retrieved from the NCBI-GEO data archive (data sets GSE153762 and GSE155622, respectively) and reanalyzed with the Seurat package (Butler et al. 2018).

Statistical analyses

Unpaired two-tailed t-test was applied for the pairwise comparison between two groups. One-way ANOVA with Dunnett's multiple comparisons posttest was performed for multigroup comparison, while two-way ANOVA with Sidak's multiple comparisons test was performed for comparison with repeated measures. All statistical analyses were performed with GraphPad Prism 9. Graphs in all figures represent mean ± SEM. Differences were considered as significant with P-values of <0.05 ($P < 0.05$ [*], $P < 0.01$ [**], and $P < 0.001$ [***]).

Competing interest statement

The authors declare no competing interests.

Acknowledgments

This project was supported by funds to H.Z. from the New York State Spinal Cord Injury Research Board (DOH01-C33268GG, DOH01-C30832GG, and DOH01-C32242GG). Y.L. and Y.W. were supported by scholarship funds from Xi'an Jiaotong University.

Author contributions: H.Z., R.H.F., X.H., and Y.L. conceived and designed the study. Y.L. and S.K. performed most experiments. Y.W., D.H., C.J.A., and F.L. supported experimental work. A.R., M.E., and L.S. analyzed RNA-seq data. Y.L., R.H.F., and H.Z. analyzed all data and wrote the manuscript. All authors discussed the results and commented on the manuscript.

References

Butler A, Hoffman P, Smibert P, Papalexi E, Satija R. 2018. Integrating single-cell transcriptomic data across different conditions, technologies, and species. *Nat Biotechnol* **36:** 411–420. doi:10.1038/nbt.4096

Cattin AL, Lloyd AC. 2016. The multicellular complexity of peripheral nerve regeneration. *Curr Opin Neurobiol* **39:** 38–46. doi:10.1016/j.conb.2016.04.005

Cattin AL, Burden JJ, Van Emmenis L, Mackenzie FE, Hoving JJ, Garcia Calavia N, Guo Y, McLaughlin M, Rosenberg LH, Quereda V, et al. 2015. Macrophage-induced blood vessels guide Schwann cell-mediated regeneration of peripheral nerves. *Cell* **162:** 1127–1139. doi:10.1016/j.cell.2015.07.021

Chen X, Nadiarynkh O, Plotnikov S, Campagnola PJ. 2012. Second harmonic generation microscopy for quantitative analysis

of collagen fibrillar structure. *Nat Protoc* **7:** 654–669. doi:10.1038/nprot.2012.009

Chen B, Chen Q, Parkinson DB, Dun XP. 2019. Analysis of Schwann cell migration and axon regeneration following nerve injury in the sciatic nerve bridge. *Front Mol Neurosci* **12:** 308. doi:10.3389/fnmol.2019.00308

Chistiakov DA, Killingsworth MC, Myasoedova VA, Orekhov AN, Bobryshev YV. 2017. CD68/macrosialin: not just a histochemical marker. *Lab Invest* **97:** 4–13. doi:10.1038/labinvest.2016.116

Conforti L, Gilley J, Coleman MP. 2014. Wallerian degeneration: an emerging axon death pathway linking injury and disease. *Nat Rev Neurosci* **15:** 394–409. doi:10.1038/nrn3680

Daviaud N, Chen K, Huang Y, Friedel RH, Zou H. 2016. Impaired cortical neurogenesis in plexin-B1 and -B2 double deletion mutant. *Dev Neurobiol* **76:** 882–899. doi:10.1002/dneu.22364

Deb Roy A, Yin T, Choudhary S, Rodionov V, Pilbeam CC, Wu YI. 2017. Optogenetic activation of Plexin-B1 reveals contact repulsion between osteoclasts and osteoblasts. *Nat Commun* **8:** 15831. doi:10.1038/ncomms15831

Dun XP, Carr L, Woodley PK, Barry RW, Drake LK, Mindos T, Roberts SL, Lloyd AC, Parkinson DB. 2019. Macrophage-derived Slit3 controls cell migration and axon pathfinding in the peripheral nerve bridge. *Cell Rep* **26:** 1458–1472.e4. doi:10.1016/j.celrep.2018.12.081

Goh FG, Piccinini AM, Krausgruber T, Udalova IA, Midwood KS. 2010. Transcriptional regulation of the endogenous danger signal tenascin-C: a novel autocrine loop in inflammation. *J Immunol* **184:** 2655–2662. doi:10.4049/jimmunol.0903359

Gonzalez-Martinez T, Perez-Piñera P, Díaz-Esnal B, Vega JA. 2003. S-100 proteins in the human peripheral nervous system. *Microsc Res Tech* **60:** 633–638. doi:10.1002/jemt.10304

Gurrapu S, Tamagnone L. 2016. Transmembrane semaphorins: multimodal signaling cues in development and cancer. *Cell Adh Migr* **10:** 675–691. doi:10.1080/19336918.2016.1197479

Jung S, Aliberti J, Graemmel P, Sunshine MJ, Kreutzberg GW, Sher A, Littman DR. 2000. Analysis of fractalkine receptor CX_3CR1 function by targeted deletion and green fluorescent protein reporter gene insertion. *Mol Cell Biol* **20:** 4106–4114. doi:10.1128/MCB.20.11.4106-4114.2000

Kalinski AL, Yoon C, Huffman LD, Duncker PC, Kohen R, Passino R, Hafner H, Johnson C, Kawaguchi R, Carbajal KS, et al. 2020. Analysis of the immune response to sciatic nerve injury identifies efferocytosis as a key mechanism of nerve debridement. *Elife* **9:** e60223. doi:10.7554/eLife.60223

Kumanogoh A, Kikutani H. 2013. Immunological functions of the neuropilins and plexins as receptors for semaphorins. *Nat Rev Immunol* **13:** 802–814. doi:10.1038/nri3545

Kuter DJ, Bain B, Mufti G, Bagg A, Hasserjian RP. 2007. Bone marrow fibrosis: pathophysiology and clinical significance of increased bone marrow stromal fibres. *Br J Haematol* **139:** 351–362. doi:10.1111/j.1365-2141.2007.06807.x

Li X, Balagam R, He TF, Lee PP, Igoshin OA, Levine H. 2017. On the mechanism of long-range orientational order of fibroblasts. *Proc Natl Acad Sci* **114:** 8974–8979. doi:10.1073/pnas.1707210114

Liu P, Peng J, Han GH, Ding X, Wei S, Gao G, Huang K, Chang F, Wang Y. 2019. Role of macrophages in peripheral nerve injury and repair. *Neural Regen Res* **14:** 1335–1342. doi:10.4103/1673-5374.253510

Maier V, Jolicoeur C, Rayburn H, Takegahara N, Kumanogoh A, Kikutani H, Tessier-Lavigne M, Wurst W, Friedel RH. 2011. Semaphorin 4C and 4G are ligands of plexin-B2 required in cerebellar development. *Mol Cell Neurosci* **46:** 419–431. doi:10.1016/j.mcn.2010.11.005

Marcolino AM, Barbosa RI, das Neves LM, Mazzer N, de Jesus Guirro RR, de Cássia Registro Fonseca M. 2016. Assessment of functional recovery of sciatic nerve in rats submitted to low-level laser therapy with different fluences. An experimental study: laser in functional recovery in rats. *J Hand Microsurg* **5:** 49–53. doi:10.1007/s12593-013-0096-0

Mehta V, Pang KL, Rozbesky D, Nather K, Keen A, Lachowski D, Kong Y, Karia D, Ameismeier M, Huang J, et al. 2020. The guidance receptor plexin D1 is a mechanosensor in endothelial cells. *Nature* **578:** 290–295. doi:10.1038/s41586-020-1979-4

Navarro X. 2009. Neural plasticity after nerve injury and regeneration. *Int Rev Neurobiol* **87:** 483–505. doi:10.1016/S0074-7742(09)87027-X

Nixon RA, Shea TB. 1992. Dynamics of neuronal intermediate filaments: a developmental perspective. *Cell Motil Cytoskeleton* **22:** 81–91. doi:10.1002/cm.970220202

Park D, Wershof E, Boeing S, Labernadie A, Jenkins RP, George S, Trepat X, Bates PA, Sahai E. 2020. Extracellular matrix anisotropy is determined by TFAP2C-dependent regulation of cell collisions. *Nat Mater* **19:** 227–238. doi:10.1038/s41563-019-0504-3

Parkhurst CN, Yang G, Ninan I, Savas JN, Yates JR III, Lafaille JJ, Hempstead BL, Littman DR, Gan WB. 2013. Microglia promote learning-dependent synapse formation through brain-derived neurotrophic factor. *Cell* **155:** 1596–1609. doi:10.1016/j.cell.2013.11.030

Parrinello S, Napoli I, Ribeiro S, Wingfield Digby P, Fedorova M, Parkinson DB, Doddrell RD, Nakayama M, Adams RH, Lloyd AC. 2010. Ephb signaling directs peripheral nerve regeneration through Sox2-dependent Schwann cell sorting. *Cell* **143:** 145–155. doi:10.1016/j.cell.2010.08.039

Rosenberg AF, Isaacman-Beck J, Franzini-Armstrong C, Granato M. 2014. Schwann cells and deleted in colorectal carcinoma direct regenerating motor axons towards their original path. *J Neurosci* **34:** 14668–14681. doi:10.1523/JNEUROSCI.2007-14.2014

Scarpa E, Roycroft A, Theveneau E, Terriac E, Piel M, Mayor R. 2013. A novel method to study contact inhibition of locomotion using micropatterned substrates. *Biol Open* **2:** 901–906. doi:10.1242/bio.20135504

Seijffers R, Mills CD, Woolf CJ. 2007. ATF3 increases the intrinsic growth state of DRG neurons to enhance peripheral nerve regeneration. *J Neurosci* **27:** 7911–7920. doi:10.1523/JNEUROSCI.5313-06.2007

Shin JE, Geisler S, DiAntonio A. 2014. Dynamic regulation of SCG10 in regenerating axons after injury. *Exp Neurol* **252:** 1–11. doi:10.1016/j.expneurol.2013.11.007

Wang H, Wu M, Zhan C, Ma E, Yang M, Yang X, Li Y. 2012. Neurofilament proteins in axonal regeneration and neurodegenerative diseases. *Neural Regen Res* **7:** 620–626.

Wang K, Wang S, Chen Y, Wu D, Hu X, Lu Y, Wang L, Bao L, Li C, Zhang X. 2021. Single-cell transcriptomic analysis of somatosensory neurons uncovers temporal development of neuropathic pain. *Cell Res* **31:** 904–918. doi:10.1038/s41422-021-00479-9

Watabe K, Fukuda T, Tanaka J, Honda H, Toyohara K, Sakai O. 1995. Spontaneously immortalized adult mouse Schwann cells secrete autocrine and paracrine growth-promoting activities. *J Neurosci Res* **41:** 279–290. doi:10.1002/jnr.490410215

Ydens E, Amann L, Asselbergh B, Scott CL, Martens L, Sichien D, Mossad O, Blank T, De Prijck S, Low D, et al. 2020. Profiling peripheral nerve macrophages reveals two macrophage subsets with distinct localization, transcriptome and response to injury. *Nat Neurosci* **23:** 676–689. doi:10.1038/s41593-020-0618-6

Yuan A, Rao MV, Veeranna, Nixon RA. 2017. Neurofilaments and neurofilament proteins in health and disease. *Cold Spring Harb Perspect Biol* **9:** a018309. doi:10.1101/cshperspect.a018309

Zhou Y, Gunput RA, Pasterkamp RJ. 2008. Semaphorin signaling: progress made and promises ahead. *Trends Biochem Sci* **33:** 161–170. doi:10.1016/j.tibs.2008.01.006

Zhou X, Wahane S, Friedl MS, Kluge M, Friedel CC, Avrampou K, Zachariou V, Guo L, Zhang B, He X, et al. 2020. Microglia and macrophages promote corralling, wound compaction and recovery after spinal cord injury via plexin-B2. *Nat Neurosci* **23:** 337–350. doi:10.1038/s41593-020-0597-7

Zigmond RE. 2012. Cytokines that promote nerve regeneration. *Exp Neurol* **238:** 101–106. doi:10.1016/j.expneurol.2012.08.017

Zochodne DW. 2012. The challenges and beauty of peripheral nerve regrowth. *J Peripher Nerv Syst* **17:** 1–18. doi:10.1111/j.1529-8027.2012.00378.x

Macrophages facilitate peripheral nerve regeneration by organizing regeneration tracks through Plexin-B2

Yuhuan Li, Sangjo Kang, Dalia Halawani, et al.

Genes Dev. 2022, **36:** originally published online January 27, 2022
Access the most recent version at doi:10.1101/gad.349063.121